Supplementary Information

Development of a force field for the simulation of single-chain proteins and protein-protein complexes

Atom	Charge		Sigma		Epsilon	
	Amber99	**DES-Amber**	**Amber99**	**DES-Amber**	**Amber99**	**DES-Amber**
Ca	0.0337	0.0337	3.400	3.353	0.1094	0.102306
Ha	0.0823	0.0823	2.471	1.540	0.0157	0.007516
C	0.5973	0.451975	3.400	3.400	0.0860	0.0860
O	−0.5679	−0.593742	2.960	3.090	0.2100	0.267428
N	−0.4157	−0.278592	3.250	3.400	0.1700	0.164024
H	0.2719	0.305959	1.069	0.000	0.0157	0.000

Table S1. Nonbonded parameters for the protein backbone atoms (kcal mol^{-1}; Å; units of charge).

Atom	Sigma			Epsilon		
	Amber99	**DES-Amber**	**DES-Amber SF1.0**	**Amber99**	**DES-Amber**	**DES-Amber SF1.0**
Na	3.328	3.410	2.084	0.00277	0.0010	0.1684
K	4.736	4.736	2.783	$3.28\ 10^{-4}$	$3.28\ 10^{-4}$	0.2795
Cl	3.400	3.451	4.718	0.0860	1.000	0.0117
O2	2.960	2.960	3.600	0.2100	0.2100	0.0200
N3	3.250	3.800	3.033	0.1700	0.0100	0.2795
NR	3.250	3.3507	3.150	0.1700	0.1700	0.1700
HN	1.0691	1.070	1.070	0.0157	0.0157	0.0157
OP	2.960	3.117	3.117	0.2100	0.2100	0.2100
OR	3.000	3.157	3.157	0.1700	0.1700	0.1700

Table S2. Revised nonbonded parameters for atoms that are part of charged groups or ions (kcal mol^{-1}; Å; units of charge).

Solute	**Concentration**	**Experiment**	**DES-Amber**
NaCl	0.5	0.921[1]	0.81(1)
	1.0	0.936	0.75(3)
	2.0	0.984	0.71(1)
KCl	0.5	0.900[1]	0.88(1)
	1.0	0.898	0.91(2)
	2.0	0.912	0.91(1)
Ace Na^+	0.5	0.958[2]	0.91(2)
	1.0	1.001	0.95(1)
	2.0	1.090	1.05(1)
Ace K^+	0.5	0.967[2]	0.96(2)
	1.0	1.018	1.10(6)
	2.0	1.124	1.13(1)
DMP Na^+	0.3	0.98[3]	0.96(2)
	0.5	1.01	0.98(2)
	1.0	1.09	1.05(2)
DMP K^+	0.3	0.98[3]	0.98(2)
	0.6	1.02	1.00(2)
	1.0	1.10	1.10(2)
NH_4Cl	0.5	0.900[1]	0.84(2)
	1.0	0.897	0.85(2)
	2.0	0.908	0.85(1)

NH_4ClO_4	0.5	0.853[1]	0.81(1)
	1.0	0.820	0.75(1)
	2.0	0.777	0.70(1)
GLY	0.5	0.956[4]	0.91(3)
	1.0	0.927	0.87(2)
	2.0	0.901	0.84(2)
ALA	0.5	1.005[5]	1.00(2)
	1.0	1.009	1.02(1)
	2.0	1.017	1.01(2)
ALA_2	0.3	0.993[6]	0.99(3)
	0.6	1.011	0.98(2)
	1.0	1.041	1.02(3)
VAL	0.3	1.023[5]	1.06(4)
	0.6	1.046	1.10(2)
SER	0.5	0.940[7]	0.95(2)
	1.0	0.915	0.92(2)
	2.0	0.900	0.92(1)
THR	0.5	0.988[8]	0.98(3)
	1.0	0.982	1.04(2)
	2.0	0.978	1.08(2)
ARG	0.5	0.785[9]	0.70(2)
	1.0	0.733	0.63(1)

	2.0	0.695	0.59(1)
LYS	0.5	0.844[9]	0.87(3)
	1.0	0.844	0.86(2)
	2.0	0.896	0.92(1)
Glu Na^+	0.5	0.907[10]	0.84(3)
	1.0	0.921	0.86(2)
	2.0	0.992	0.91(1)
Glu K^+	0.5	0.922[10]	0.93(2)
	1.0	0.948	1.01(2)
	2.0	1.035	1.13(1)

Table S3. Comparison of calculated and experimental osmotic coefficients for DES-Amber

Atom Pair	Experiment	DES-Amber
Na - Cl	~2.8[11,12] (crystal)	2.65
Na - O_{wat}	2.3[13,14]	2.45
Cl - O_{wat}	3.2[13,15]	3.15
K - Cl	~3.0[12] (crystal)	3.00
K - O_{wat}	2.7[13]	2.80
NH_4 - O_{wat}	2.8-3.0[15,16]	2.8
NH_4 - Cl	~3.2-3.3[15,17]	3.1

Table S4. Comparison of calculated and experimental position of the first peak of the Radial Distribution Function (Å).

Residue	PDB distribution			DES-Amber			RMSD
	-	+	t	-	+	t	
ARG	0.54	0.04	0.43	0.41	0.01	0.58	0.12
ASN	0.80	0.01	0.19	0.62	0.01	0.37	0.15
ASP	0.79	0.02	0.19	0.83	0.00	0.17	0.03
CYS	0.75	0.05	0.20	0.65	0.03	0.33	0.10
GLN	0.61	0.04	0.35	0.53	0.00	0.46	0.08
GLU	0.61	0.01	0.38	0.42	0.01	0.57	0.15
HIS	0.52	0.00	0.48	0.32	0.01	0.67	0.16
ILE	0.92	0.05	0.03	0.97	0.00	0.03	0.04
LEU	0.66	0.01	0.33	0.57	0.00	0.43	0.08
LYS	0.54	0.00	0.46	0.41	0.00	0.59	0.10
MET	0.72	0.02	0.26	0.57	0.00	0.42	0.13
PHE	0.41	0.01	0.58	0.32	0.00	0.68	0.08
SER	0.44	0.33	0.22	0.42	0.43	0.14	0.07
THR	0.75	0.25	0.00	0.78	0.22	0.00	0.03
TRP	0.39	0.03	0.58	0.23	0.03	0.74	0.13
TYR	0.42	0.01	0.57	0.34	0.00	0.66	0.07
VAL	0.07	0.02	0.91	0.12	0.06	0.81	0.07

Table S5. Side-chain χ_1 rotamer distributions as obtained from 1-μs simulations of Ace-A_4XA_4-Nma peptides restrained to helical conformations compared to the distributions observed in the PDB for residues in α helices.[18]

AA	NMR experiment			DES-Amber		
	278K	298K	333K	278K	298K	333K
Ala	1.56	1.39	1.17	1.70	1.38	1.12
Cys	0.37	0.36	0.59	0.62	0.55	0.50
Asp	0.56	0.54	0.94	0.93	0.74	0.69
Glu	1.22	1.00	1.04	1.47	1.20	1.04
Phe	0.52	0.50	0.72	0.80	0.67	0.59
Gly	0.17	0.22	0.51	0.32	0.28	0.29
His	0.18	0.20	0.31	0.59	0.51	0.55
Ile	0.78	0.81	0.98	0.80	0.72	0.87
Lys	0.67	0.60	0.67	0.51	0.42	0.44
Leu	1.10	1.15	1.22	1.44	1.38	1.48
Met	0.87	0.90	0.99	0.95	0.83	0.78
Asn	0.37	0.43	0.75	0.69	0.58	0.55
Pro	0.01	0.05	0.31	0.01	0.01	0.01
Gln	0.68	0.72	0.86	1.01	0.91	0.92
Arg	0.97	0.80	0.70	1.43	1.25	0.98
Ser	0.45	0.51	0.83	0.87	0.71	0.68
Thr	0.36	0.40	0.71	0.70	0.59	0.63
Val	0.55	0.53	0.78	0.47	0.40	0.49
Trp	0.53	0.64	0.92	0.59	0.61	0.83
Tyr	0.50	0.50	0.72	0.67	0.55	0.57

Table S6. Lifson-Roig helix extension parameters at three temperatures (278 K, 298 K, and 333 K) as obtained from fitting the helical fractions observed in a 20-μs simulated tempering simulation of Ace-$(AAXAA)_3$-Nme peptides compared to the experimental values obtained from NMR experiments.[19]

Ubq	***a99SB*-disp**	***DES-Amber SF1.0***	***DES-Amber***
BB 3J	1.16	1.16	1.14
HB 3J	0.14	0.13	0.13
BB RDCs	0.26	0.22	0.22
SC RDCs	0.41	0.41	0.40
SC3J	1.06	1.11	1.17
Amide S2	0.04	0.06	0.06
Methyl S2	0.11	0.14	0.14
Score	***1.37***	***1.47***	***1.46***
GB3	**a99SB-*disp***	**DES-Amber SF1.0**	**DES-Amber**
BB 3J	1.35	1.01	1.01
Hbond 3J	0.17	0.12	0.12
BB RDCs	0.23	0.14	0.15
SC 3J	1.12	1.05	1.01
Amide S2	0.05	0.03	0.04
Score	***1.44***	***1.03***	***1.05***
HEWL	**a99SB-*disp***	**DES-Amber SF1.0**	**DES-Amber**
RDC	0.39	0.29	0.32
SC 3J	1.02	1.00	1.06
Amide S2	0.06	0.06	0.05
Methyl S2	0.19	0.20	0.18
Score	***1.15***	***1.06***	***1.06***
BPTI	**a99SB-*disp***	**DES-Amber SF1.0**	**DES-Amber**
BB 3J	1.00	1.22	1.21
SC 3J	1.00	1.21	1.25
BB RDC	0.45	0.40	0.40
Score	***1.04***	***1.15***	***1.16***

Table S7. Comparison between simulation and NMR experimental data for the four folded proteins in the Robustelli benchmark. RMSDs from experiments are reported in Hz for the scalar couplings of backbone (BB 3J), side chain (SC 3J) and through-hydrogen bond (HB 3J); for amide (Amide S2 and Methyl (Methyl S2) order parameters, the unitless RMSD is reported, and for backbone (BB RDC) and side-chain (SC RDC) RDCs, the unitless Q-score is reported. The deviations and force field scores (Score) are only reported for DES-Amber, DES-Amber

SF1.0, and a99SB-*disp*, but were calculated for each type of experimental observable also taking into account previously reported simulations[20] run using a99SB-*disp*, a99SB*-ILDN/TIP3P, c22*/TIP3P, c36m/TIP3P, a03ws, a99SB-UCB, and a99SB-ILDN/TIP4P-D.

drkN SH3	a99SB-disp	DES-Amber SF1.0	DES-Amber
CA	0.50	0.97	0.51
HA	0.10	0.22	0.13
HN	0.23	0.32	0.20
C	0.65	0.88	0.60
CB	0.50	1.04	0.54
RDC Q	0.91	1.00	0.94
Rg	19.46	15.13	18.86
PRE	0.30	0.27	0.24
BB 3J	0.70	1.20	0.66
R	0.40	0.23	0.61
Score	***1.19***	***1.65***	***1.13***
ACTR	**a99SB-*disp***	**DES-Amber SF1.0**	**DES-Amber**
CA	0.46	0.70	0.59
HA	0.18	0.16	0.18
N	0.87	1.15	0.90
C	0.42	0.54	0.45
CB	0.30	0.43	0.37
RDC Q	0.81	0.96	0.79
Rg	21.29	16.77	20.10
PRE	0.22	0.18	0.20
Score	***1.18***	***1.50***	***1.26***
Ntail	**a99SB-*disp***	**DES-Amber SF1.0**	**DES-Amber**
CA	0.44	0.67	0.69
HN	0.12	0.17	0.18
N	0.89	1.22	1.30
C	0.41	0.64	0.68
CB	0.37	0.73	0.58
RDC Q	0.95	0.97	1.00
Rg	26.65	19.12	21.91
Score	***1.01***	***1.58***	***1.48***
Asyn	**a99SB-*disp***	**DES-Amber SF1.0**	**DES-Amber**
CA	0.51	0.60	0.33
HN	0.14	0.17	0.11
N	1.46	1.75	1.21
C	0.31	0.52	0.40
CB	1.04	1.25	1.13
RDC Q	0.41	0.61	0.35

Rg	36.76	18.76	30.54
PRE	0.17	0.27	0.18
3J HNHA	1.11	0.98	0.73
R	0.56	0.39	0.76
3J SC	0.18	0.27	0.22
R	0.19	0.29	0.45
sigma	3.40	4.01	2.82
R	0.25	0.30	0.40
Score	***1.28***	***1.83***	***1.11***
PaaA2	**a99SB-*disp***	**DES-Amber SF1.0**	**DES-Amber**
CA	0.64	0.95	0.71
HA	0.10	0.13	0.12
HN	0.17	0.18	0.13
N	0.99	1.49	1.00
C	0.66	0.64	0.58
CB	0.37	0.53	0.43
RDC Q	0.76	0.47	0.61
Rg	21.39	14.36	18.63
Score	***1.35***	***1.37***	***1.19***
Abeta	**a99SB-*disp***	**DES-Amber SF1.0**	**DES-Amber**
CA	0.47	0.55	0.33
HA	0.09	0.14	0.08
HN	0.29	0.30	0.25
N	1.54	1.34	0.80
CB	0.40	0.59	0.40
RDC Q	0.50	0.61	0.51
Rg	13.91	13.18	17.13
3J HNHA	0.64	0.82	0.67
R	0.63	0.55	0.76
Score	***1.28***	***1.49***	***1.40***
GCN4	**a99SB-*disp***	**DES-Amber SF1.0**	**DES-Amber**
CA	0.65	0.77	0.54
HN	0.24	0.24	0.25
N	0.90	1.11	0.92
C	0.60	0.64	0.53
Amide S2	0.07	0.34	0.14
Score	***1.04***	***3.03***	***1.52***
p15AF	**Amber-*disp***	**DES-Amber SF1.0**	**DES-Amber**

CA	0.40	0.46	0.38
HA	0.07	0.15	0.13
HN	0.14	0.17	0.15
N	0.72	1.18	1.03
C	0.36	0.42	0.36
CB	0.36	0.5	0.4
RDC Q	0.74	0.76	0.73
Rg	27.2	19.4	27.1
Score	***1.06***	***1.58***	***1.18***
Ash1	**Amber-*disp***	**DES-Amber SF1.0**	**DES-Amber**
CA	0.45	0.27	0.31
HA	0.11	0.18	0.16
N	1.06	0.83	0.71
HN	0.53	0.53	0.51
C	0.41	0.52	0.45
Rg	31.6	25.5	27.2
Score	***1.24***	***1.23***	***1.14***
Sic1	**Amber-*disp***	**DES-Amber SF1.0**	**DES-Amber**
CA	0.77	0.61	0.63
HA	0.22	0.27	0.26
HN	0.12	0.14	0.13
N	1.17	0.86	0.78
CB	0.52	0.64	0.59
RDC Q	0.43	0.42	0.44
Rg	24.42	25.0	23.0
Score	***1.31***	***1.27***	***1.32***

Table S8. Comparison between simulation and experimental data for the 10 disordered proteins in the Robustelli benchmark. RMSDs from experiments are reported in Hz for the chemical shifts of atoms Cα (CA), Hα (HA), HN (HN), N (N), and Cβ (CB); the radius of gyration (Rg) is reported in Å; for scalar couplings (3J), the RMSD in Hertz is reported, as well as the correlation coefficient (R); for amide order parameters (Amide S2) and PREs (PRE), the unitless RMSD is reported, and for RDCs, the unitless Q-score is reported (RDC Q). The deviations and force field scores (Score) are only reported for DES-Amber, DES-Amber SF1.0 and a99SB-*disp*, but

were calculated for each type of experimental observable also taking into account previously reported simulations[20] run using a99SB-*disp*, a99SB*-ILDN/TIP3P, c22*/TIP3P, c36m/TIP3P, a03ws, a99SB-UCB, and a99SB-ILDN/TIP4P-D.

	DES-Amber	DES-Amber SF1.0	a99SB-*disp*	NMR structure
Cα CS	1.05	1.07	1.07	2.84
Hα CS	0.26	0.27	0.27	0.50
HN CS	0.47	0.48	0.47	0.63
C' CS	1.41	1.43	1.40	2.02
Cβ CS	1.10	1.12	1.10	5.01
HN CS	2.61	2.63	2.60	2.96
CS FF Score	**1.00**	**1.02**	**1.01**	**2.16**
Average # of NOE violations	85.6	87.6	92.6	54.6
NOEs RMSD from experiment	0.49	0.50	0.55	0.30
NOE FF Score	**1.00**	**1.02**	**1.10**	**0.63**

Table S9. Comparison of calculated RMSD from experimental chemical shift measurements and number of NOE violations for 10-μs simulations of 41 proteins described in Mao et al.[21] Chemical shift RMSDs (CS) are reported in ppm. NOE violations are defined as interatomic distances that exceed distance restraints by >1 Å. Agreement with experimental values obtained from the lowest energy NMR structure is shown for comparison, but FF scores are calculated using only the agreement observed in MD simulations. FF scores are only reported for DES-Amber, DES-Amber SF1.0, and a99SB-*disp*, but were calculated for each type of experimental observable also taking into account previously reported simulations[20] run using a99SB-*disp*, a99SB*-ILDN/TIP3P, c22*/TIP3P, C36m/TIP3P, a03ws, a99SB-UCB, and a99SB-ILDN/TIP4P-D.

	DES-Amber	DES-Amber SF1.0	a99SB-*disp*	Experiment
drKN SH3	18.8	15.1	19.5	16.7 ± 1.4
ACTR	20.1	16.8	21.3	25.0 ± 1.0
N_{TAIL}	21.9	19.1	26.7	27.5 ± 0.7
α-synuclein	30.5	18.8	36.8	31.0 ± 5.0
PaaA2	18.6	14.3	21.4	22.4 ± 4.0
Aβ40	17.1	13.2	13.9	12.0 ± 1.3
$p15^{PAF}$	27.0	19.4	27.2	28.1 ± 0.3
Ash1	27.2	25.5	24.4	28.5 ± 3.4
Sic1	23.0	25.0	31.6	32.1 ± 0.8
Calmodulin	20.7	19.1	21.5	21.5 ± 1.0
Average % Error	9.7%	15.6%	5.1%	

Table S10. Comparison of the simulated and experimental radii of gyration (R_gs) for the disordered proteins of the Robustelli benchmark simulated in this work.

Trp-cage variant	# events	ΔG_{sim}	ΔG_{exp}
Tc10b	82	-0.43±0.14	-0.57±0.31[22,23]
Tc10b D1N	78	0.00±0.12	-0.26±0.02[22]
Tc10b A2L	84	-0.14±0.12	0.05±0.12[22]
Tc10b Y3A	35	1.72±0.17	2.53±0.20[22]
Tc10b Y3F	87	-0.10±0.12	-0.01±0.25[22]
Tc10b Y3L	81	0.02±0.12	0.49±0.15[22]
Tc10b A4I	94	-0.41±0.14	-0.32±0.19[22]
Tc10b D1N/Q5A	76	0.19±0.12	0.36±0.06[22]
Tc10b W6F	35	2.20±0.19	2.41±0.25[24]
Tc10b L7A	42	1.17±0.14	2.22±0.74[22]
Tc10b K8A	71	-0.22±0.17	-0.94±0.25[22]
Tc10b D9N	169	-0.07±0.07	0.24±0.50[22]
Tc10b P12A	98	-0.12±0.12	0.24±0.25[22]
Tc10b S13A	64	-0.14±0.12	-1.00±0.31[22]
Tc10b S14A	100	0.48±0.10	1.54±0.74[22]
Tc10b S14T	87	0.12±0.12	0.30±0.25[22]
Tc10b R16K	128	0.05±0.12	0.11±0.19[22,23,25]
Tc10b P17A	100	0.19±0.12	0.30±0.31[22]
Tc10b P18A	68	-0.19±0.12	-0.01±0.19[22]
Tc10b P19A	82	1.60±0.12	1.97±0.16[22,23]
Tc5b	86	-0.41±0.12	0.30±0.19[22,26]
Tc5b P12W	68	0.07±0.14	-0.63±0.05[27]

Table S11. Reversible folding simulations of 22 variants of the Trp-cage miniprotein using the DES-Amber force field. For each variant, the number of folding events (# events) and the calculated (ΔG_{sim}) and experimental (ΔG_{exp}) folding free energies (kcal mol^{-1}) are reported.

Name	**a99SB*-ILDN**	**c22***	**RSFF2 +**	**c36m**	**a99SB-*disp***	**DES-Amber**
Ubq/UEV	2.7	*13.7*	*17.2*	2.6	1.4	**1.3**
Insulin dimer	4.0	4.6	5.0	3.5	3.8	**2.8**
Ubq/Ubq-ligase	**1.3**	*8.4*	4.1	*8.5*	*3.9*	2.6
TβR-1/FKBP12	2.8	5.1	3.3	3.1	3.6	**2.7**
Pex5p/SCP2	3.8	4.1	2.8	5.9	3.3	**2.7**
BPTI/MT-SP1	2.3	2.2	2.6	2.3	1.8	**1.6**
SGPB/OMTKY 3	2.2	5.0	**1.7**	2.5	*14.0*	2.4
Barnase/Barstar	**2.3**	*14.5*	*8.9*	4.5	*10.5*	**2.3**
BPTI/Trypsin	**1.6**	2.1	2.4	3.2	1.9	2.9

Table S12. MD simulations of nine protein complexes with different force fields. The table reports the average Cα RMSD (Å) of the complex calculated over the last microsecond of a 20-μs simulation. The lowest average RMSD among all force fields is highlighted in bold; simulations in which the complex dissociated are highlighted in italics. Aside from DES-Amber, the only other force field that accurately reproduced the structure of these nine protein complexes was a99SB*-ILDN with TIP3P water, possibly because this force field has the tendency to overstabilize compact conformations.

Name	Pk_{diss} (s^{-1})	a99SB*-ILDN	RSFF2+	c36m	a99SB-*disp*	DES-Amber
Ubq/UEV	>2[28]	-	4.5	-	-	-
Insulin dimer	4.0[29]	-	-	-	-	-
Ubq/Ubq-ligase	*1.8*[30]	-	4.9	5.5	4.7	-
TβR-1/FKBP12	*0.5*[31]	-	-	-	-	-
Pex5p/SCP2	-3.2[32]	-	-	-	-	-
BPTI/MT-SP1	*-4.3*[33]	-	4.9	-	-	-
SGPB/OMTKY3	*-3.2*[34]	-	-	-	-	-
Barnase/Barstar	-5[35]	-	4.4	-	5.4	-
BPTI/Trypsin	-7.2[36]	-	-	-	-	-

Table S13. Base-10 logarithm of the dissociation rates for 9 protein-protein complexes from MD simulations performed with different force fields. The dissociation rates estimated from simulation are compared to the experimental values. Experimental values in italics are estimates based on the experimental equilibrium constant and assuming a diffusion-limited association constant of 10^6 s^{-1} M^{-1}.[37] If no calculated value is reported, no dissociation was observed in any of the two 20-μs simulations, indicating a dissociation rate smaller than 10^5 s^{-1} ($Pk_{diss} < 5$).

Name	PDB entry	ΔG_{bind} (kcal mol^{-1} M^{-1})	ΔG_{bind} (a99SB-*disp)*	ΔG_{bind} (DES-Amber)	ΔG_{bind} (a99SB*-ILDN*)*	ΔG_{bind} (c36m*)*	Interface area (Å^2)
Ubq/UEV	1S1Q[38]	-4.3[28]	-7.8(8)	-8.2(4)	-10.2(6)	-6.8(5)	650
Insulin dimer	1TRZ[39]	-5.5[40]	-	-	-	-	800
Ubq/Ubq-ligase	2OOB[30]	-5.8[30]	-	-6.7(1)	-10(2)	-5.4(2)	450
TβR-1/FKBP12	1B6C[31]	-7.6	-19.0(5)	-13(5)	-17(2)	-12(1)	920
Pex5p/SCP2	2C0L[41]	-9.8[41]	-3(4)	-6(3)	-12(3)	-5(1)	870
BPTI/MT-SP1	1EAW[42]	-14[33]	-12(1)	-	-	-	960
SGPB/OMTKY3	3SGB[34]	-12.5[34]	-3(3)	-6(2)	-14(3)	-	660
Barnase/Barstar	1BRS[43]	-18[43]	-3(1)	-14(8)	-10(1)	-	840
BPTI/Trypsin	2PTC[44]	-18[45]	-	-	-	-	720
colE7/Im7	7CEI[38]	-19.8[46]	-10(3)	-13.0(2)	-19(6)	-	690
FAB/Factor VIII	1IQD[47]	-14.1[48]	-	-11.7(5)	-		1020
Ad12/CAR D1	1KAC[49]	-8.9[50]	-	-1.7(3)	-		760
ImGP Synthase	1GPW[51]	-7.9[52]	-	-6.4(3)	-		1070
CD2/CD58	1QA9[53]	-7.2[53]	-	-7.9(1)	-		690

Table S14. Calculated association free energies for protein-protein complexes. For the complexes where values could be obtained using two different restraint sets, the average and standard deviation of the two measurements is reported. In the other cases, the error estimated using blocking is reported. Comparison of the two sets of errors suggests that blocking has the tendency to underestimate the error, possibly because of long-timescale correlations.

Protein	DES-Amber		Experiment	
	ΔH_u (300 K)	**ΔC_p**	**ΔH_u (300 K)**	**ΔC_p**
Trp-cage	4.1(5)	0.09(1)	15.5(5)[22]	0.05(3)[22]
Villin	-2.5(3)	0.27(1)	*10*[54]	*0.3*[54]
WW-domain	6(1)	0.21(1)	-	-
BBA	0.3(5)	0.13(2)	*11(2)*[55]	-
NTL-9	-17	0.39(1)	*10(1)*[56]	*0.53(6)*[56]
BdpA	0	0.5(2)	15[57]	0.43[57]
Engrailed	2(1)	0.30(5)	15(1)[58]	-
gpW	-6(1)	0.47(1)	11[59]	0.6[59]
α3D	-4.2(5)	0.16(1)		0.8[60]
λ-repressor	-1(1)	0.30(1)		

Table S15. Thermodynamics of protein folding. Folding enthalpy (kcal mol^{-1}) at 300 K and folding heat capacity (kcal mol^{-1} K^{-1}) calculated from the ST folding simulations are compared to the experimental values. Experimental values in italics indicate that there are differences between the experimental and simulated sequence.

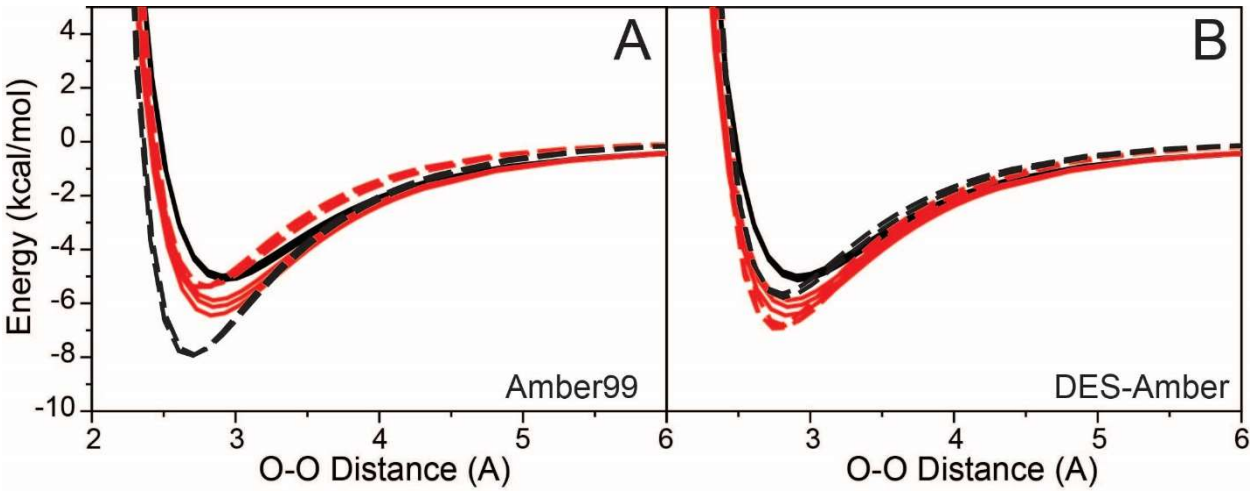

Figure S1. Comparison of interaction energies between methanol and water calculated at the MP2 (solid lines) and MM (dashed lines) level. Calculations were performed for both Amber99 (A) and DES-Amber (B). In the red traces water is acting as a hydrogen bonding donor, whereas in the black traces it is acting as an acceptor. Scans were performed for different values of the C-C-O-H torsion angle. Note that the Amber99 force field predicts the wrong relative stability for the donor and acceptor hydrogen bonds; this imbalance is corrected in DES-Amber.

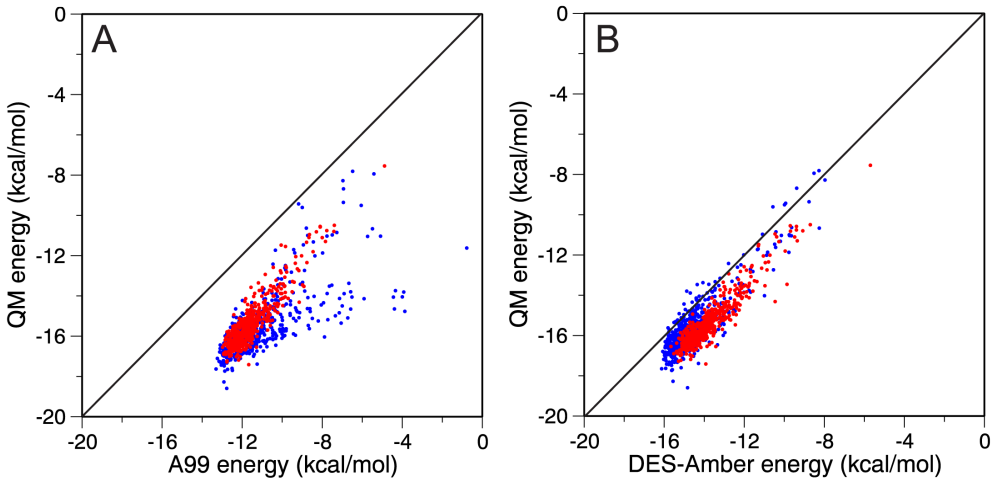

Figure S2. Interaction energies (kcal mol^{-1}) for NMA trimers taken from α-helices (red) or β-sheets (blue) calculated using the standard Amber99 force field (A) and after the nonbonded parameter optimization (B) compared to the reference MP2 data.

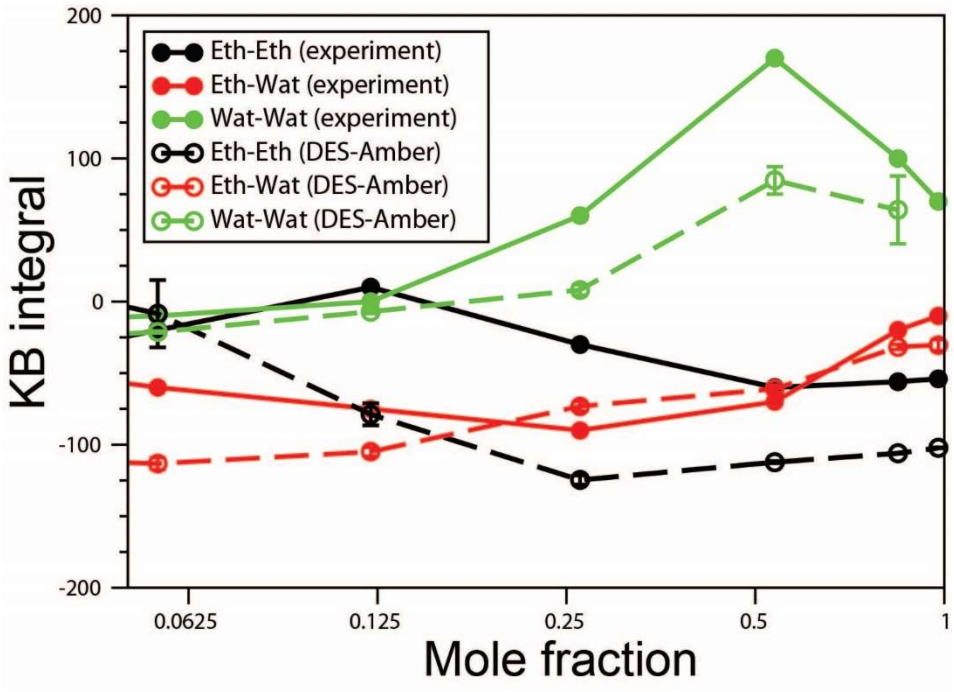

Figure S3. Kirkwood-Buff integrals for ethanol-water mixtures as a function of increasing ethanol mole fraction. Kirkwood-Buff integrals were either derived from experimental measurements[61] (solid lines) or calculated from simulations performed with the DES-Amber force field (dashed lines).

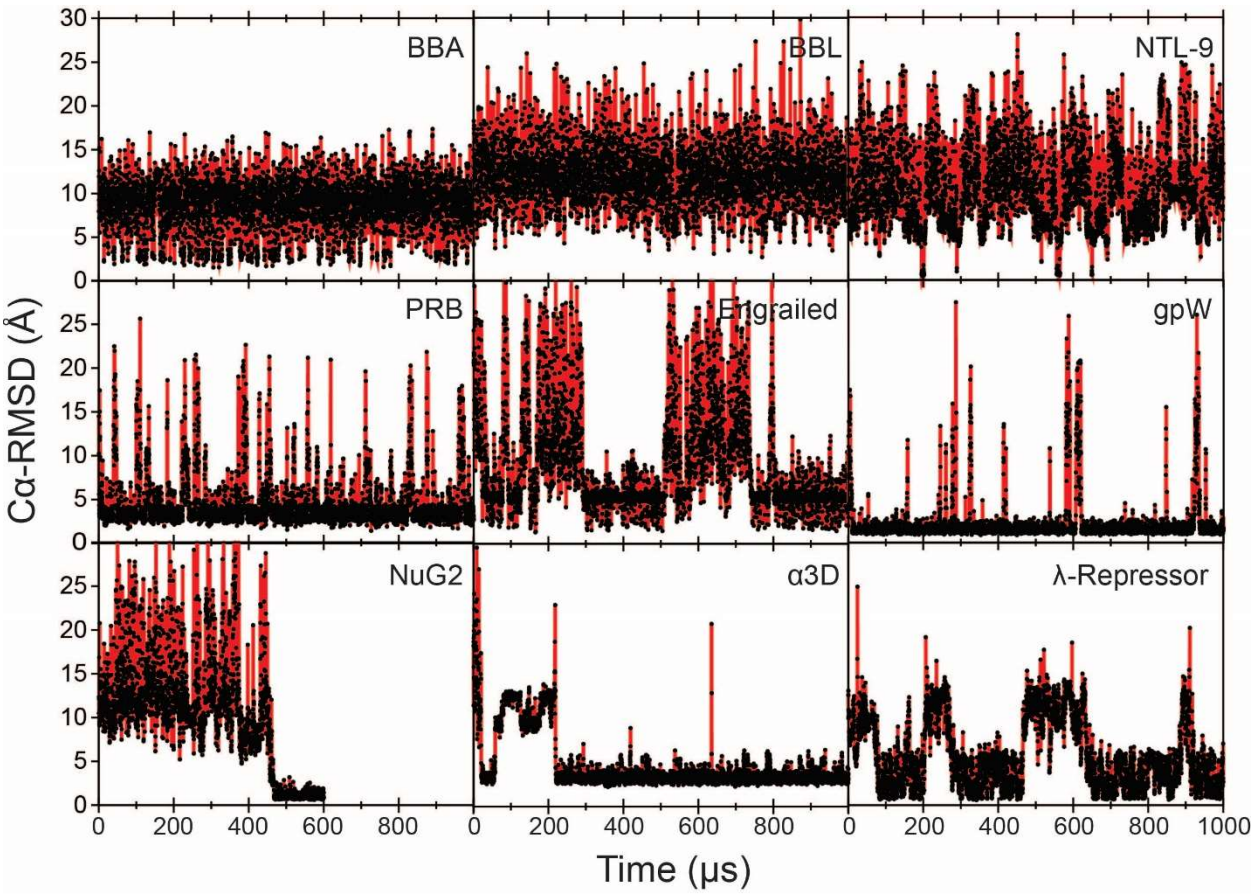

Figure S4. Simulated tempering simulations of nine fast folding proteins. Cα-RMSD traces as a function of time. For NuG2, the simulated tempering simulation did not result in any folding event (i.e., structures with a Cα-RMSD <2 Å from the folded state). The Cα-RMSD trace of an NPT simulation at 360 K is reported instead, in which the protein folded after ~500 μs of simulation.

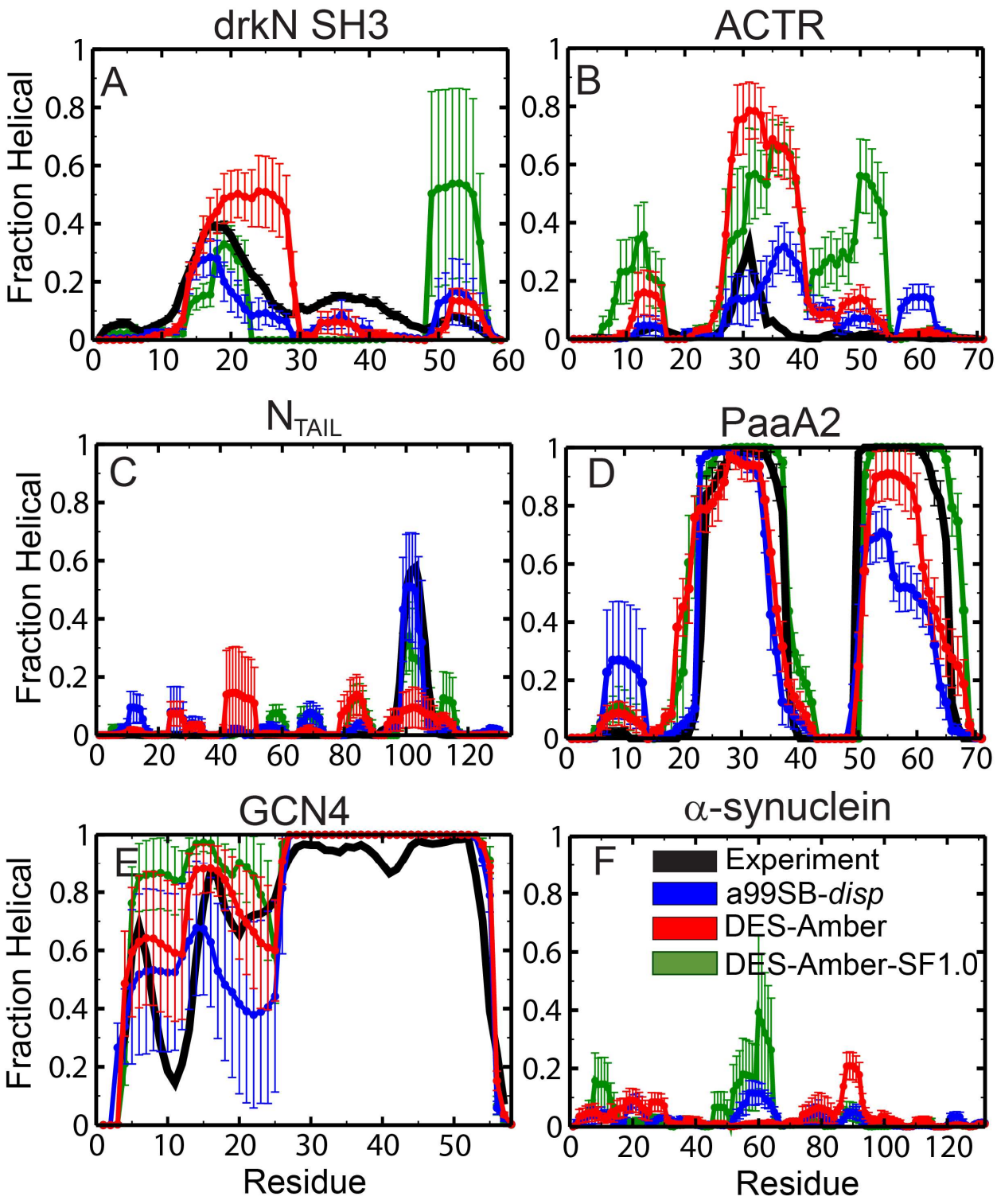

Figure S5. Helical propensities observed in simulations of the disordered proteins drkN SH3

(A), ACTR (B), N_{TAIL} (C), PaaA2 (D), GCN4 (E), and α-synuclein (F). Black lines are experimental estimates from restrained-ensemble models calculated from NMR data (drkN SH3,[62] N_{TAIL},[63] PaaA2[64]) or predicted from experimental NMR chemical shifts using the program δ2d[65] (ACTR, α-synuclein, GCN4).

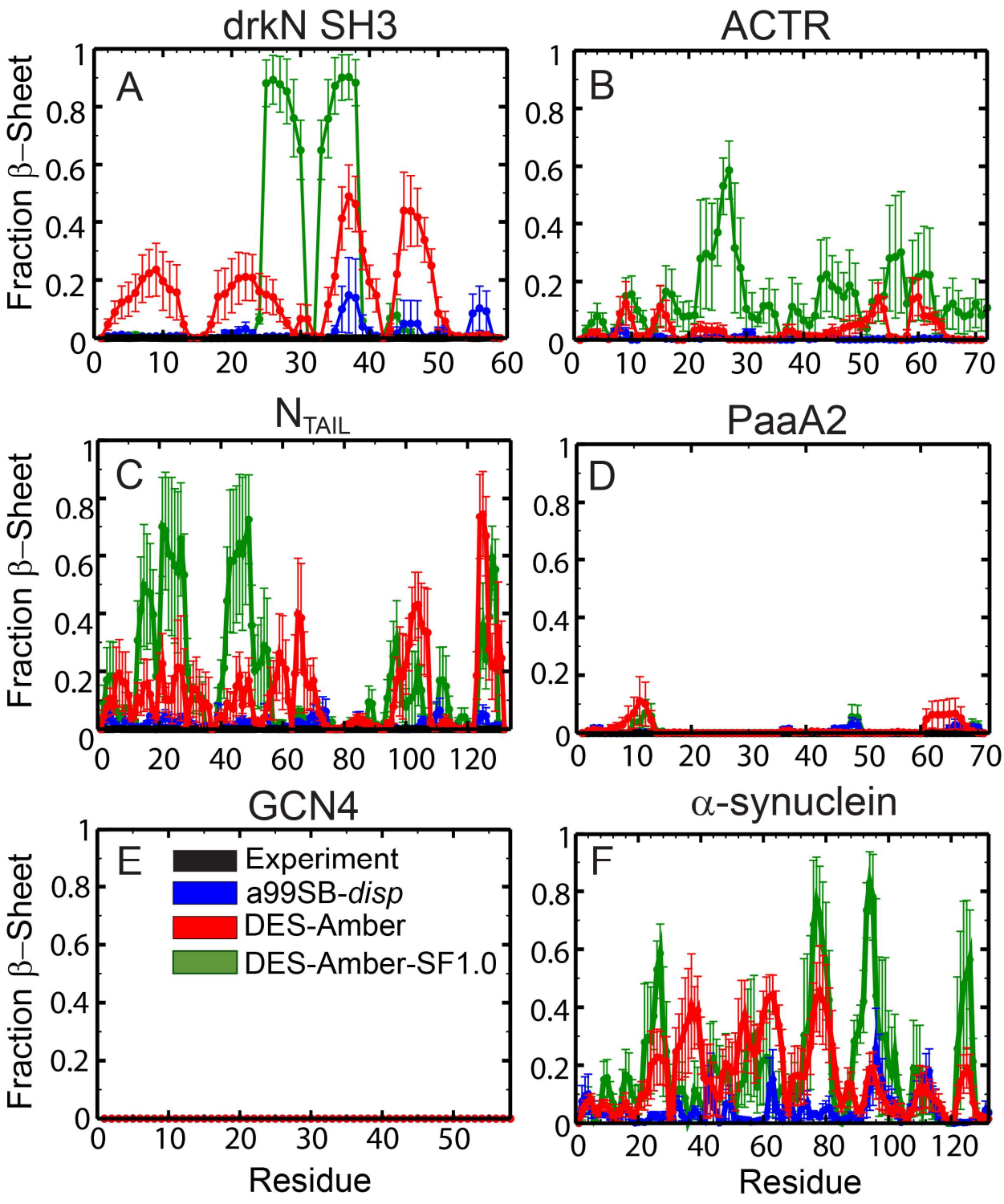

Figure S6. β-propensities observed in simulations of the disordered proteins drkN SH3 (A),

ACTR (B), N_{TAIL} (C), PaaA2 (D), GCN4 (E), and α-synuclein (F).

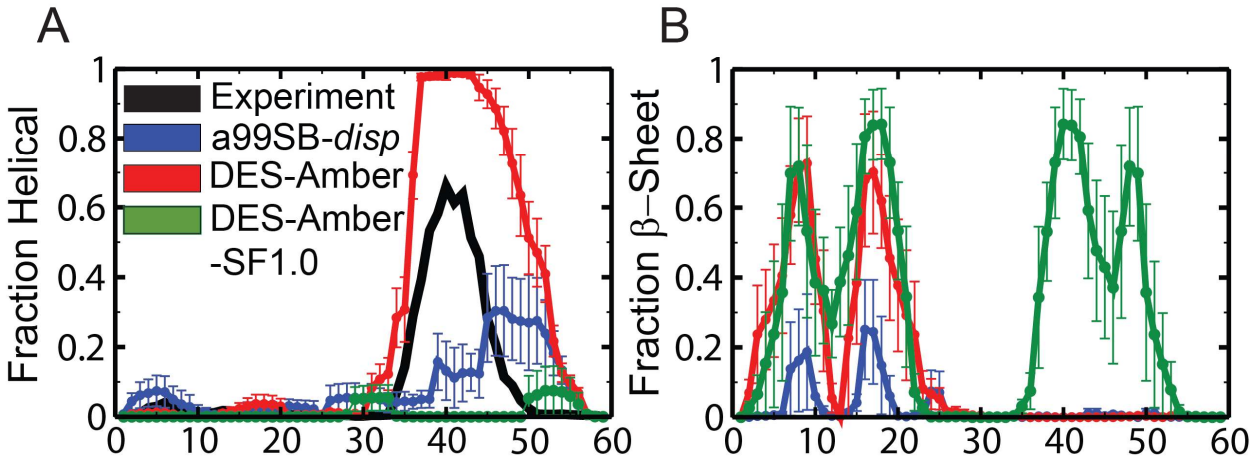

Figure S7. Helical (A) and Beta (B) propensities observed in simulations of the disordered Sendai N_{TAIL}. Black lines are experimental estimates predicted from experimental NMR chemical shifts using the program δ2d.

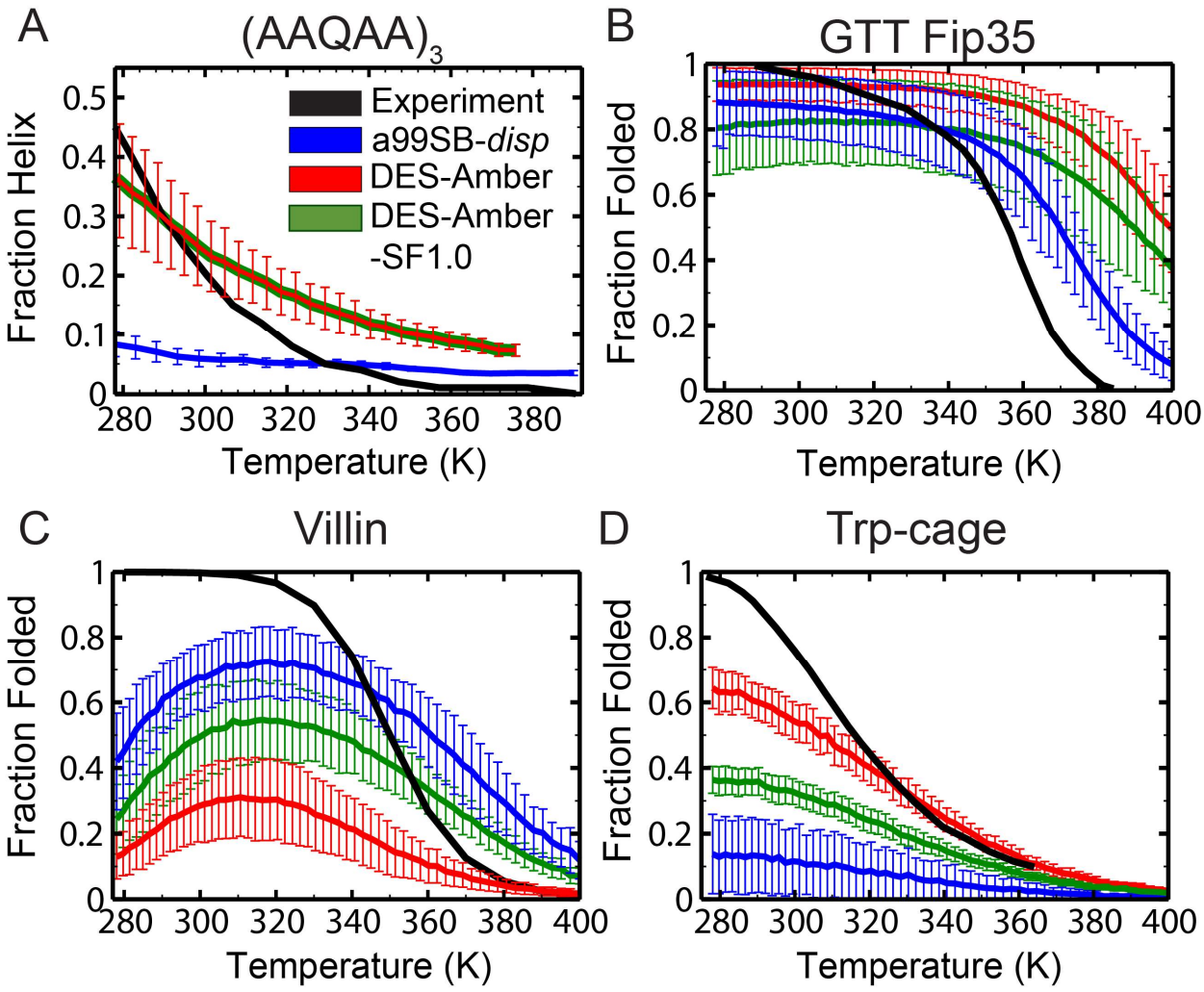

Figure S8. Thermal stability of the helical peptide $(AAQAA)_3$ (A) and the fast-folding proteins GTT-Fip35 (B) Nle-Nle villin (C) and Trp-cage (D). Experimental melting curves are shown in black.

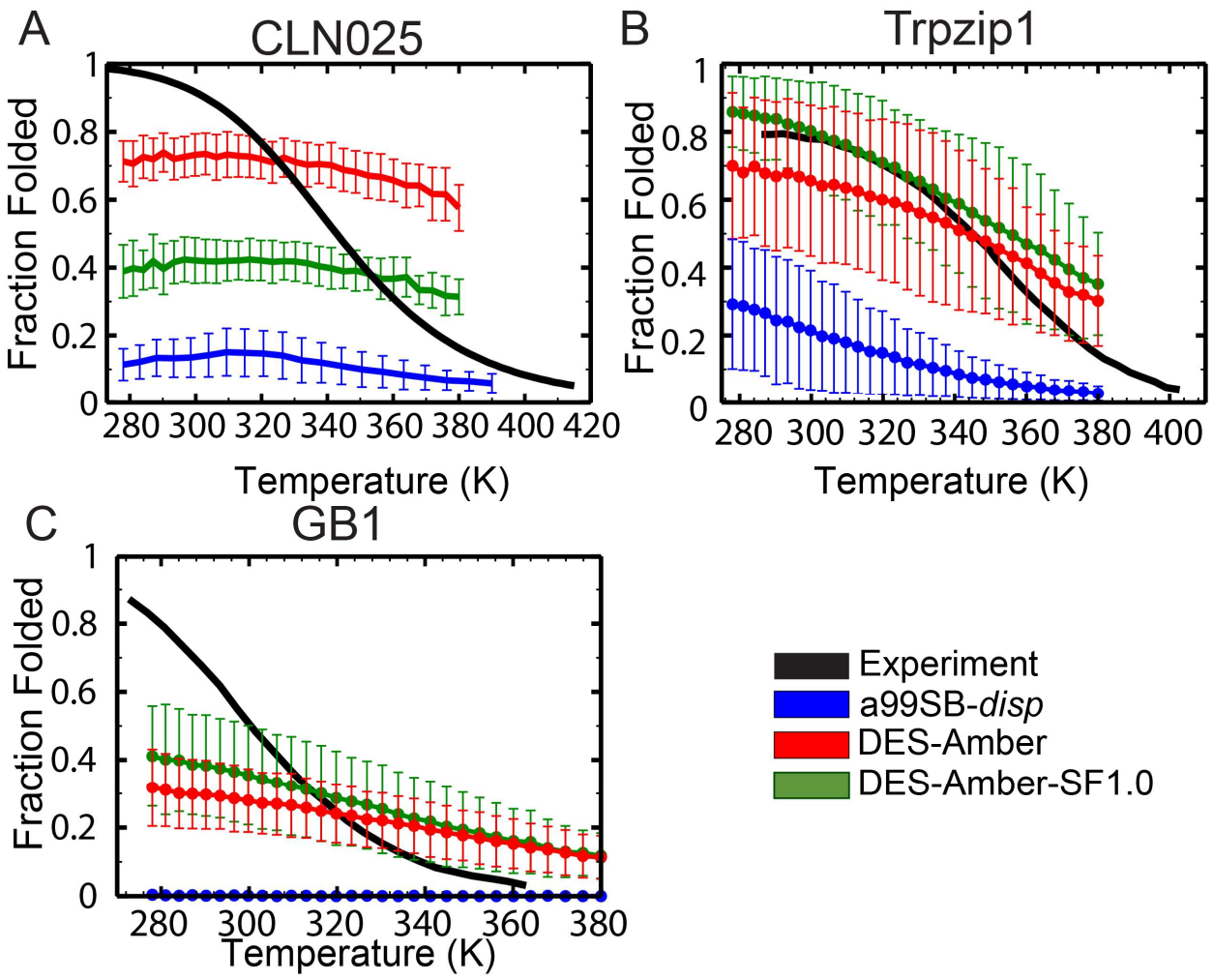

Figure S9. Thermal stability of β-hairpin forming peptides CLN025 (A), Trpzip1 (B), and the GB1 hairpin (C). Experimental melting curves are shown in black.

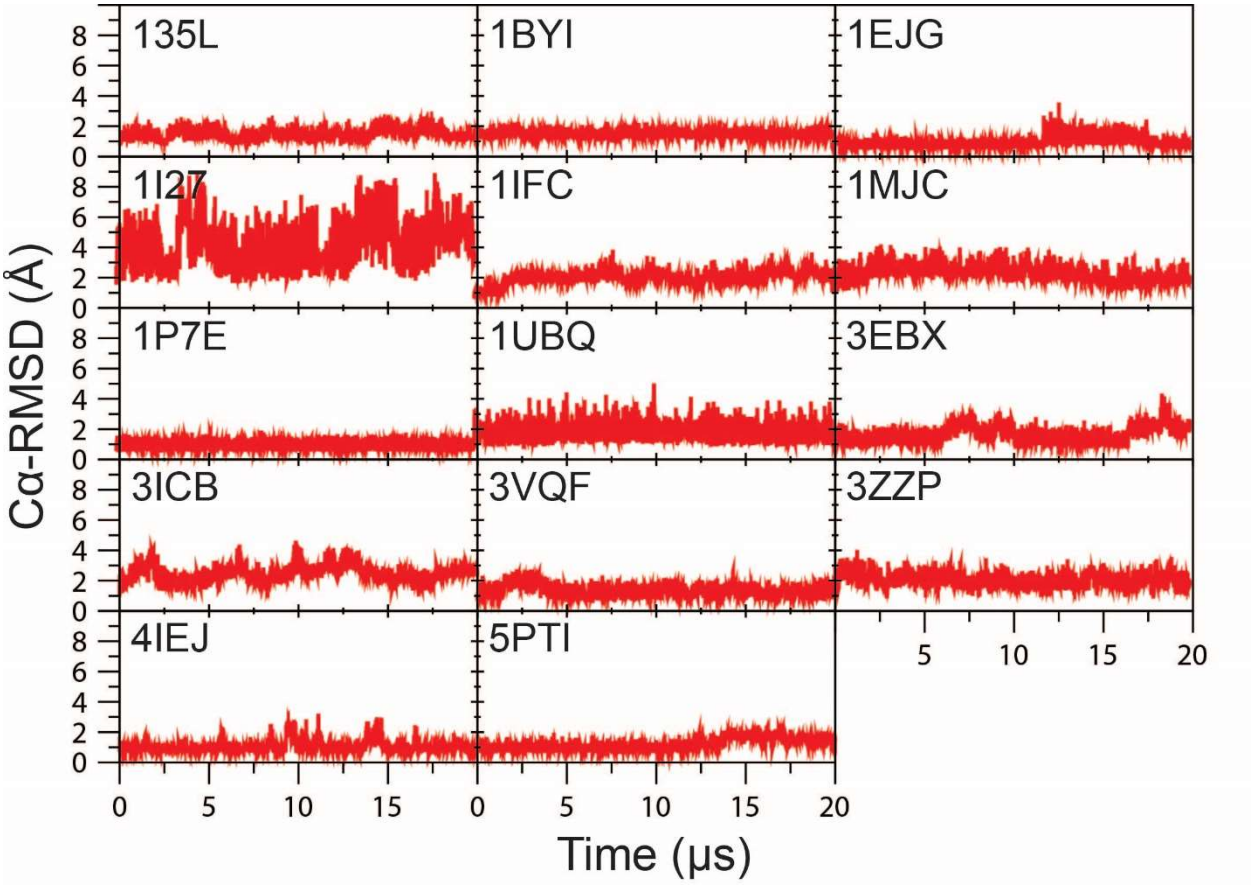

Figure S10. Cα-RMSD time series for 14 folded proteins[66] selected among the highest resolution structures in the PDB during a 20-μs simulation performed with the DES-Amber force field. For each protein, the corresponding PDB ID is reported.

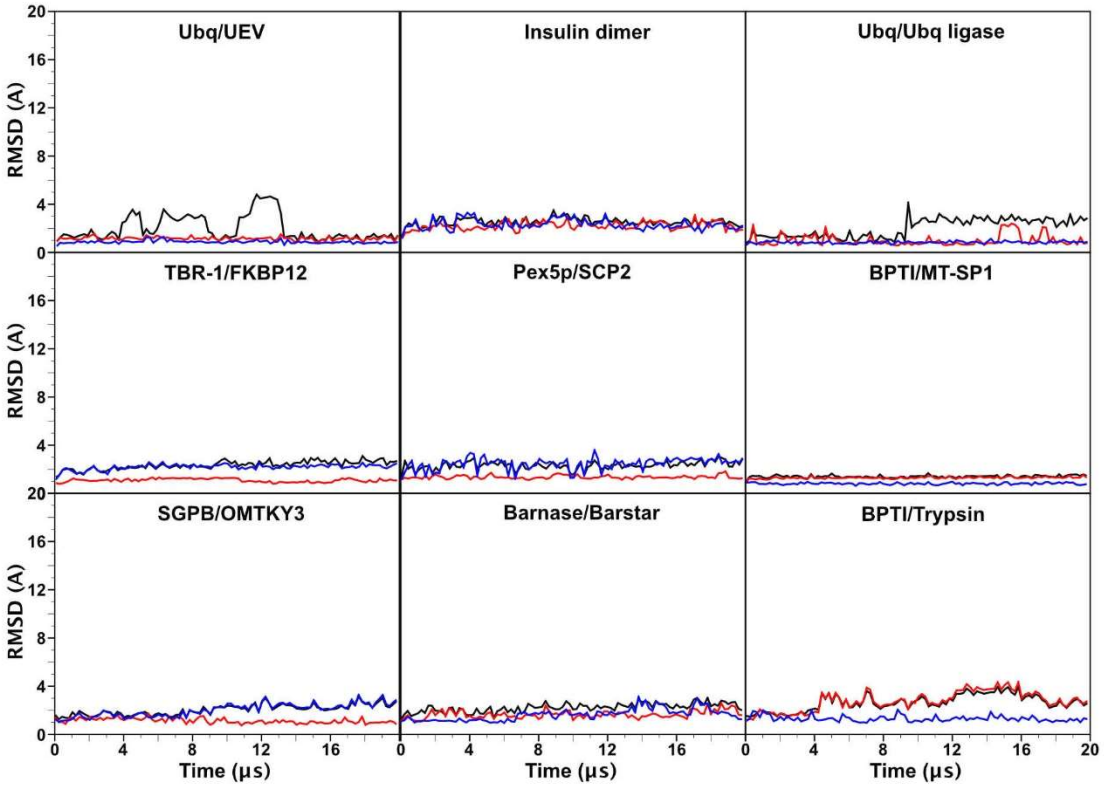

Figure S11. Cα RMSD time series plots obtained from 20-μs simulations of nine protein-protein complexes using DES-Amber. For each complex, the RMSD of each protein monomer is reported in red and blue; the RMSD of the complex is reported in black.

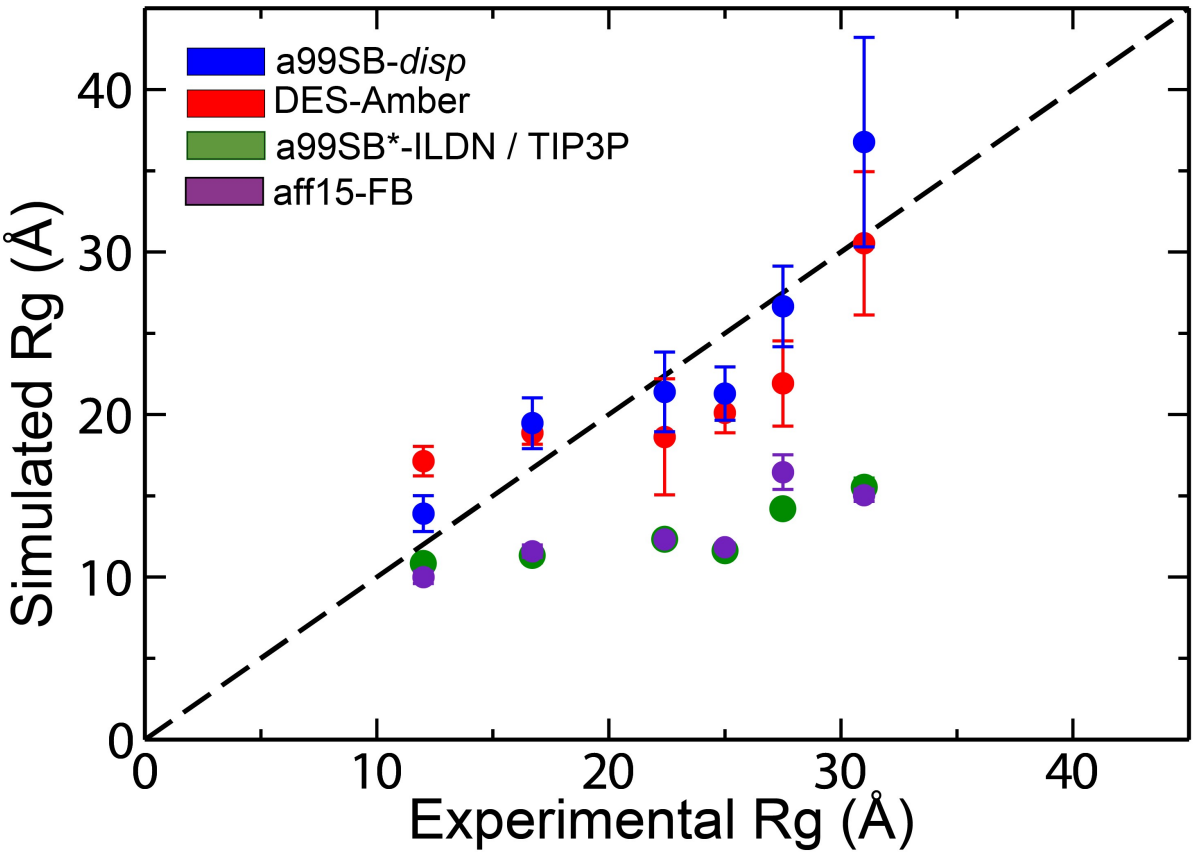

Figure S12. Comparison of the simulated and experimental radii of gyration (R_gs) for a subset of the disordered proteins (drKN SH3, ACTR, Aβ40, PaaA2, N_{TAIL}, α-synuclein) simulated in this work with a99SB-*disp*, DES-Amber, a99SB*-ILDN/TIP3P, and Amber-FB15. We note that the simulated dimensions of disordered proteins were very similar between a99SB*-ILDN/TIP3P and Amber-FB15, which utilizes the TIP3P-FB water model. The force field scores of this subset of disordered proteins with Amber-FB15 were on average slightly better than those with a99SB*-ILDN/TIP3P (1.91 vs. 2.28 for Amber-FB15 and a99SB*-ILDN/TIP3P, respectively), suggesting some improvement in the local structural features for disordered proteins.

References

1. Hamer, W. J.; Wu, Y.-C. Osmotic coefficients and mean activity coefficients of uni-univalent electrolytes in water at 25°C. *J. Phys. Chem. Ref. Data* **1972**, *1(4)*, 1047–1099.

2. Robinson, R. A. The activity coefficients of the alkali bromides and iodides in aqueous solution from vapor pressure measurements. *J. Am. Chem. Soc.* **1935**, *57(7)*, 1161–1165 .

3. Tamaki, K.; Suga, K.; Tanihara, E. Solution properties of dialkyl phosphate salts—apparent molar volumes, viscosity B-coefficients, heats of solution, and osmotic coefficients. *Bull. Chem. Soc. Jpn.* **1987**, *60*, 1225–1229.

4. Smith, E. R. B.; Smith, P. K. The activity of glycine in aqueous solution at twenty-five degrees. *J. Biol. Chem.* **1937**, *117*, 209–216.

5. Smith, P. K.; Smith, E. R. B. The activity of aliphatic amino acids in aqueous solution at 25°C. *J. Biol. Chem.* **1937**, *121*, 607–613.

6. Smith, E. R. B.; Smith, P. K. Thermodynamic properties of solutions of amino acids and related substances VI. The activities of some peptides in aqueous solution at twenty-five degrees. *J. Biol. Chem.* **1940**, *135*, 273–279.

7. Hutchens, J. O.; Figlio, K. M.; Granito, S. M. An isopiestic comparison method for activities. The activities of L-arginine–hydrochloride. *J. Biol. Chem.* **1963**, *238*, 1419–1422.

8. Smith, P. K.; Smith, E. R. B. The activities of some hydroxy- and N-methylamino acids and proline in aqueous solution at 25°C. *J. Biol. Chem.* **1940**, *132*, 57–64.

9. Bonner, O. D. Osmotic and activity coefficients of some amino acids and their hydrochloride salts at 298.15 K. *J. Chem. Eng. Data* **1982**, *27*, 422–423.

10. Bonner, O. D. Osmotic and activity coefficients of sodium and potassium glutamate at 298.15 K. *J. Chem. Eng. Data* **1981**, *26*, 147–148.

11. Nickel, J. E.; Fineman, M. A.; Wallace, W. E. X-ray diffraction studies of sodium chloride-sodium bromide solid solutions. *J. Phys. Chem.* **1949**, *53(5)*, 625–628.

12. Bragg, W. L. The structure of some crystals as indicated by their diffraction of X-rays. *Proc. R. Soc. Lond. A* **1913**, *89*, 248–277.

13. Mancinelli, R.; Botti, A.; Bruni, F.; Ricci, M. A.; Soper, A. K. Hydration of sodium, potassium, and chloride ions in solution and the concept of structure maker/breaker. *J. Phys. Chem. B* **2007**, *111(48)*, 13570–13577.

14. Xu, J.; Fang, Y.; Fang, C. Structure of aqueous sodium sulfate solutions derived from X-ray diffraction. *Chin. Sci. Bull.* **2009**, *54(12)*, 2022–2027.

15. Narten, A. H. Diffraction pattern and structure of aqueous ammonium halide solutions. *J. Phys. Chem.* **1970**, *74(4)*, 765–768.

16. Hewish, N. A.; Neilson, G. W. Ammonium ion coordination in concentrated aqueous ammonium chloride. *Chem. Phys. Lett.* **1981**, *84(3)*, 425–427.

17. Anselmo, V. C.; Smith, N. ,O. Lattice constants of ammonium chloride-ammonium bromide solid solutions. *J. Phys. Chem.* **1959**, *63*, 1344.

18. Lovell, S. C.; Word, J. M.; Richardson, J. S.; Richardson, D. C. The penultimate rotamer library. *Proteins* **2000**, *40(3)*, 389–408.

19. Moreau, R. J.; Schubert, C. R.; Nasr, K. A.; Török, M.; Miller, J. S.; Kennedy, R. J.; Kemp, D. S. Context-independent, temperature-dependent helical propensities for amino acid residues. *J. Am. Chem. Soc.* **2009**, *131(36)*, 13107–13116.

20. Robustelli, P.; Piana, S.; Shaw, D. E. Developing a molecular dynamics force field for both folded and disordered protein states. *Proc. Natl. Acad. Sci. U. S. A.* **2018**, *115(21)*, E4758–E4766.

21. Mao, B.; Tejero, R.; Baker, D.; Montelione, G. T. Protein NMR structures refined with Rosetta have higher accuracy relative to corresponding X-ray crystal structures. *J. Am. Chem. Soc.* **2014**, *136(5)*, 1893–1906.

22. Barua, B.; Lin, J. C.; Williams, V. D.; Kummler, P.; Neidigh, J. W.; Andersen, N. H. The Trp-cage: optimizing the stability of a globular miniprotein. *Protein Eng. Des. Sel.* **2008**, *21(3)*, 171–185.

23. Culik, R. M.; Serrano, A. L.; Bunagan, M. R.; Gai, F. Achieving secondary structural resolution in kinetic measurements of protein folding: A case study of the folding mechanism of Trp-cage. *Angew. Chem. Int. Ed. Engl.* **2011**, *50(46)*, 10884–10887.

24. Barua, B.; Andersen, N. H. Determinants of miniprotein stability: can anything replace a buried H-bonded Trp sidechain? *Lett. Pept. Sci.* **2002**, 8(3–5), 221–226.

25. Williams, D. V.; Byrne, A.; Stewart, J.; Andersen, N. H. Optimal salt bridge for Trp-cage stabilization. *Biochemistry* **2011**, *50*, 1143–1152.

26. Streicher, W. W.; Makhatadze, G. I. Unfolding thermodynamics of Trp-cage, a 20 residue miniprotein, studied by differential scanning calorimetry and circular dichroism spectroscopy. *Biochemistry* **2007**, *46(10)*, 2876–2880.

27. Bunagan, M. R.; Yang, X.; Saven, J. G.; Gai, F. Ultrafast folding of a computationally designed Trp-cage mutant: Trp2-cage. *J. Phys. Chem. B* **2006**, *110(8)*, 3759–3763.

28. Pornillos, O.; Alam, S. L.; Rich, R. L.; Myszka, D. G.; Davis, D. R.; Sundquist, W. I. Structure and functional interactions of the Tsg101 UEV domain. *EMBO J.* **2002**, *21(10)*, 2397–2406.

29. Koren, R.; Hammes, G. G. A kinetic study of protein-protein interactions. *Biochemistry* **1976**, *15(5)*, 1165–1171.

30. Peschard, P.; Kozlov, G.; Lin, T.; Mirza, I. A.; Berghuis, A. M.; Lipkowitz, S.; Park, M.; Gehring, K. Structural basis for ubiquitin-mediated dimerization and activation of the ubiquitin protein ligase Cbl-b. *Mol. Cell* **2007**, *27(3)*, 474–485.

31. Huse, M.; Chen, Y. G.; Massagué, J.; Kuriyan, J. Crystal structure of the cytoplasmic domain of the type I TGF beta receptor in complex with FKBP12. *Cell* **1999**, *96(3)*, 425–436.

32. Williams, C. P.; Schueller, N.; Thompson, C. A.; van den Berg, M.; van Haren, S. D.; Erdmann, R.; Bond, C. S.; Distel, B.; Schliebs, W.; Wilmanns, M.; Stanley, W. A. The Peroxisomal Targeting Signal 1 in sterol carrier protein 2 is autonomous and essential for receptor recognition. *BMC Biochem.* **2011**, *12*, 12.

33. Farady, C. J.; Sun, J.; Darragh, M. R.; Miller, S. M.; Craik, C. S. The mechanism of inhibition of antibody-based inhibitors of membrane-type serine protease 1 (MT-SP1). *J. Mol. Biol.* **2007**, *369(4)*, 1041–1051.

34. Read, R. J.; Fujinaga, M.; Sielecki, A. R.; James, M. N. Structure of the complex of Streptomyces griseus protease B and the third domain of the turkey ovomucoid inhibitor at 1.8-Å resolution. *Biochemistry* **1983**, *22(19)*, 4420–4433.

35. Schreiber, G.; Fersht, A. R. Interaction of barnase with its polypeptide inhibitor barstar studied by protein engineering. *Biochemistry* **1993**, *32(19)*, 5145–5150.

36. Vincent, J. P.; Lazdunski, M. Trypsin-pancreatic trypsin inhibitor association. Dynamics of the interaction and role of disulfide bridges. *Biochemistry* **1972**, *11(16)*, 2967–2977.

37. Schreiber, G.; Haran, G.; Zhou, H. X. Fundamental aspects of protein-protein association kinetics. *Chem. Rev.* **2009**, *109(3)*, 839–860.

38. Sundquist, W. I.; Schubert, H. L.; Kelly, B. N.; Hill, G. C.; Holton, J. M.; Hill, C. P. Ubiquitin recognition by the human TSG101 protein. *Mol. Cell* **2004**, *13(6)*, 783–789.

39. Ciszak, E.; Smith, G. D. Crystallographic evidence for dual coordination around zinc in the T3R3 human insulin hexamer. *Biochemistry* **1994**, *33(6)*, 1512–1517.

40. Lord, R. S.; Gubensek, F.; Rupley, J. A. Insulin self-association. Spectrum changes and thermodynamics. *Biochemistry* **1973**, *12(22)*, 4385–4391.

41. Stanley, W. A.; Filipp, F. V.; Kursula, P.; Schüller, N.; Erdmann, R.; Schliebs, W.; Sattler, M.; Wilmanns, M. Recognition of a functional peroxisome type 1 target by the dynamic import receptor pex5p. *Mol. Cell* **2006**, *24(5)*, 653–663.

42. Friedrich, R.; Fuentes-Prior, P.; Ong, E.; Coombs, G.; Hunter, M.; Oehler, R.; Pierson, D.; Gonzalez, R.; Huber, R.; Bode, W.; Madison, E. L. Catalytic domain structures of MT-SP1/Matriptase, a matrix-degrading transmembrane serine proteinase. *J. Biol. Chem.* **2002**, *277*, 2160–2168.

43. Buckle, A. M.; Schreiber, G.; Fersht, A. R. Protein-protein recognition: Crystal structural analysis of a barnase-barstar complex at 2.0-Å resolution. *Biochemistry* **1994**, *33(30)*, 8878–8889.

44. Marquart, M.; Walter, J.; Deisenhofer, J.; Bode, W.; Huber, R. The geometry of the reactive site and of the peptide groups in trypsin, trypsinogen and its complexes with inhibitors. *Acta Crystallogr. Sect. B* **1983**, *39*, 480–490.

45. Vincent, J. P.; Lazdunski, M. Trypsin-pancreatic trypsin inhibitor association. Dynamics of the interaction and role of disulfide bridges. *Biochemistry* **1972**, *11(16)*, 2967–2977.

46. Keeble, A. H.; Kirkpatrick, N.; Shimizu, S.; Kleanthous, C. Calorimetric dissection of colicin DNase–immunity protein complex specificity. *Biochemistry* **2006**, *45(10)*, 3243–3254.

47. Spiegel, P. C., Jr.; Jacquemin, M.; Saint-Remy, J. M.; Stoddard, B. L.; Pratt, K. P. Structure of a factor VIII C2 domain-immunoglobulin G4kappa Fab complex: Identification of an inhibitory antibody epitope on the surface of factor VIII. *Blood* **2001**, *98(1)*, 13–19.

48. Jacquemin, M. G.; Desqueper, B. G.; Benhida, A.; Vander Elst, L.; Hoylaerts, M. F.; Bakkus, M.; Thielemans, K.; Arnout, J.; Peerlinck, K.; Gilles, J. G.; Vermylen, J.; Saint-Remy, J. M. Mechanism and kinetics of factor VIII inactivation: Study with an IgG4 monoclonal antibody derived from a hemophilia A patient with inhibitor. *Blood* **1998**, *92(2)*, 496–506.

49. Bewley, M. C.; Springer, K.; Zhang, Y. B.; Freimuth, P.; Flanagan, J. M. Structural analysis of the mechanism of adenovirus binding to its human cellular receptor, CAR. *Science* **1999**, *286(5444)*, 1579–1583.

50. Howitt, J.; Bewley, M. C.; Graziano, V.; Flanagan, J. M.; Freimuth, P. Structural basis for variation in adenovirus affinity for the cellular coxsackievirus and adenovirus receptor. *J. Biol. Chem.* **2003**, *278(28)*, 26208–26215.

51. Douangamath, A.; Walker, M.; Beismann-Driemeyer, S.; Vega-Fernandez, M. C.; Sterner, R.; Wilmanns, M. Structural evidence for ammonia tunneling across the (βα)8 barrel of the imidazole glycerol phosphate synthase bienzyme complex. *Structure* **2002**, *10(2)*, 185–193.

52. Kastritis, P. L.; Bonvin, A. M. Are scoring functions in protein-protein docking ready to predict interactomes? Clues from a novel binding affinity benchmark. *J. Proteome Res.* **2010**, *9(5)*, 2216–2225.

53. Wang, J. H.; Smolyar, A.; Tan, K.; Liu, J. H.; Kim, M.; Sun, Z. Y.; Wagner, G.; Reinherz, E. L. Structure of a heterophilic adhesion complex between the human CD2 and CD58 (LFA-3) counterreceptors. *Cell* **1999**, *97(6)*, 791–803.

54. Kubelka, J.; Henry, E. R.; Cellmer, T.; Hofrichter, J.; Eaton, W. A. Chemical, physical, and theoretical kinetics of an ultrafast folding protein. *Proc. Natl. Acad. Sci. U. S. A.* **2008**, *105(48)*, 18655–18662.

55. Feng, J. A.; Kao, J.; Marshall, G. R. A second look at mini-protein stability: analysis of FSD-1 using circular dichroism, differential scanning calorimetry, and simulations. *Biophys. J.* **2009**, *97(10)*, 2803–2810.

56. Kuhlman, B.; Raleigh, D. P. Global analysis of the thermal and chemical denaturation of the N-terminal domain of the ribosomal protein L9 in H2O and D2O. Determination of the thermodynamic parameters, deltaH(o), deltaS(o), and deltaC(o)p and evaluation of solvent isotope effects. *Protein Sci.* **1998**, *7(11)*, 2405–2412.

57. Dimitriadis, G.; Drysdale, A.; Myers, J. K.; Arora, P.; Radford, S. E.; Oas, T. G.; Smith, D. A. Microsecond folding dynamics of the F13W G29A mutant of the B domain of staphylococcal protein A by laser-induced temperature jump. *Proc. Natl. Acad. Sci. U. S. A.* **2004**, *101(11)*, 3809–3814.

58. Mayor, U.; Johnson, C. M.; Daggett, V.; Fersht, A. R. Protein folding and unfolding in microseconds to nanoseconds by experiment and simulation. *Proc. Natl. Acad. Sci. U. S. A.* **2000**, *97(25)*, 13518–13522.

59. Fung, A.; Li, P.; Godoy-Ruiz, R.; Sanchez-Ruiz, J. M.; Muñoz, V. Expanding the realm of ultrafast protein folding: gpW, a midsize natural single-domain with α+β topology that folds downhill. *J. Am. Chem. Soc.* **2008**, *130(23)*, 7489–7495.

60. Walsh, S. T.; Cheng, H.; Bryson, J. W.; Roder, H.; DeGrado, W. F. Solution structure and dynamics of a de novo designed three-helix bundle protein. *Proc. Natl. Acad. Sci. U. S. A.* **1999**, *96(10)*, 5486–5491.

61. Ben-Naim, A. Inversion of the Kirkwood-Buff theory of solutions: Application to the water-ethanol system. *J. Chem. Phys.* **1977**, *67*, 4884–4890.

62. Marsh, J. A.; Forman-Kay, J. D. Structure and disorder in an unfolded state under nondenaturing conditions from ensemble models consistent with a large number of experimental restraints. *J. Mol. Biol.* **2009**, *391(2)*, 359–374.

63. Ozenne, V.; Schneider, R.; Yao, M.; Huang, J. R.; Salmon, L.; Zweckstetter, M.; Jensen, M. R.; Blackledge, M. Mapping the potential energy landscape of intrinsically disordered proteins at amino acid resolution. *J. Am. Chem. Soc.* **2012**, *134(36)*, 15138–15148.

64. Sterckx, Y. G.; Volkov, A. N.; Vranken, W. F.; Kragelj, J.; Jensen, M. R.; Buts, L.; Garcia-Pino, A.; Jové, T.; van Melderen, L.; Blackledge, M.; van Nuland, N. A.; Loris, R. Small-angle X-ray scattering-and nuclear magnetic resonance-derived conformational ensemble of the highly flexible antitoxin PaaA2. *Structure* **2014**, *22(6)*, 854–865.

65. Camilloni, C.; De Simone, A.; Vranken, W. F.; Vendruscolo, M. Determination of secondary structure populations in disordered states of proteins using nuclear magnetic resonance chemical shifts. *Biochemistry* **2012**, *51(11)*, 2224–2231.

66. Huang, J.; Rauscher, S.; Nawrocki, G.; Ran, T.; Feig, M.; de Groot, B. L.; Grubmüller, H.; MacKerell, A. D., Jr. CHARMM36m: an improved force field for folded and intrinsically disordered proteins. *Nat. Methods.* **2017**, *14(1)*, 71–73.